CRYSTAL PRECIPITATION AND DISSOLUTION IN A POROUS MEDIUM: EFFECTIVE EQUATIONS AND NUMERICAL EXPERIMENTS*

T. L. VAN NOORDEN†

Abstract. We investigate a two-dimensional microscale model for crystal dissolution and precipitation in a porous medium. The model contains a free boundary and allows for changes in the pore volume. Using a level set formulation of the free boundary, we apply a formal homogenization procedure to obtain upscaled equations. For general microscale geometries, the homogenized model that we obtain falls in the class of distributed microstructure models. For circular initial inclusions the distributed microstructure model reduces to a system of partial differential equations coupled with an ordinary differential equation. In order to investigate how well the upscaled equations describe the behavior of the microscale model, we perform numerical computations for a test problem. The numerical simulations show that for the test problem the solution of the homogenized equations agrees very well with the averaged solution of the microscale model.

1. Introduction. In this paper we use a formal limiting procedure with asymptotic expansions to derive a macroscopic law for crystal dissolution and precipitation in a porous medium. The microscopic model that serves as the starting point for the limiting process incorporates the change in volume of the pore space as a result of the precipitation/dissolution process. In [17], the same microscopic model is considered in a thin strip. In the present paper we investigate the model on a perforated domain.

Macroscopic laws for reactive transport in porous media, which include the present case of crystal dissolution and precipitation, are of practical importance in many physical, biological, and chemical applications. Macroscopic laws for reactive transport in porous media are derived rigorously in, e.g., [6]. For the more specific case of crystal dissolution and precipitation, macroscopic models are given in [3, 4, 7, 8]. In these papers the macroscopic models presented are analyzed but are not supported by a rigorous derivation. In most of these papers the numerical solution of the proposed model equations is also studied. Related work, in which the transport of dissolved material is analyzed, can be found in [14, 16].

The main difficulty in performing the formal homogenization for the crystal dissolution and precipitation reaction is that the equations that describe the microscale processes contain a free boundary. This free boundary describes the interface between the layer of crystalline solid attached to the grains and the fluid occupying the pores. The location of this free boundary is an unknown in the model and moves with speed proportional to the local dissolution/precipitation rate. The microscale model with the free boundary has been studied in [18] in a one-dimensional setting and without

†Department of Mathematics and Computer Science, Technische Universiteit Eindhoven, P.O. Box 513, 5600 MB Eindhoven, The Netherlands (T.L.v.Noorden@tue.nl).

flow. Other works that study crystal dissolution and precipitation on the microscale are [12] and [13].

The crystal dissolution and precipitation problem has also been studied in [7] and [15, 19]. The main difference between the cited papers and the present paper is that in the cited papers it is assumed that the thickness of the layer of crystalline solid attached to the grains domain is negligible so that the pore geometry can be assumed to be fixed. In this case the formal homogenization is a rather standard procedure and the macroscopic equations can be derived straightforwardly.

In this paper we do take into account the change in the pore volume due to the precipitation/dissolution reaction. For the microscale model this results in a free boundary problem, and for the macroscopic model this results in a permeability and porosity that depend on the local pore geometry. The behavior of solutions of the microscale model are numerically studied using the arbitrary Lagrangian–Eulerian method. The structure of this paper is as follows. In section 2 we will discuss the model equations that describe the processes at the microscale. In section 3 we will derive using a formal limiting argument the effective equations for the limit of the pore size tending to zero, and in section 4 we show that the effective model can be simplified for certain initial configurations. In section 5 the numerical results for both the microscale model and the effective equations are presented and compared.

2. Model equations. We consider the same model for crystal dissolution and precipitation as described in [17]. In this paper, however, we consider a different microscale geometry of the porous medium. The porous medium is in the present paper represented by a two-dimensional perforated domain. We denote the two-dimensional bounded domain by Ω, with boundary Γ, and we suppose that the grains of the porous medium are circles. Let the centers of the circles B_{ij}, all with radius $R_g < \epsilon/2$, be located in an equidistant grid with nodes at $(\epsilon i, \epsilon j)$, where ϵ is a small dimensionless length scale. This periodic distribution of the grains is, of course, not very realistic, but it is frequently made in homogenization theory [5] in order to derive macroscopic models which are then also used for more general situations.

The pore space is completely occupied by a fluid which contains dissolved solutes (ions) which can precipitate on the grain boundary and form a crystalline solid, the precipitate. The reverse reaction of dissolution is also possible. We consider only one solute (the cation), even though dissolution and precipitation involve another species, the anion. This is a simplified setting that is also considered in [17, 18], which can be achieved by considering another quantity, the total electric charge (see [7, 15]). Under appropriate boundary and initial conditions, the total charge remains constant in time and space, and the two species have equal concentrations. The boundary that is the interface between the crystalline solid that surrounds the circle B_{ij} and the pore space is denoted by $\Gamma_{ij}(t)$, with normal ν^ϵ, pointing into the crystalline phase, and its normal velocity is denoted by v_n^ϵ (see Figure 1). The dimensionless equation for the normal velocity is given by (see [17])

$$(2.1) \qquad v_n^\epsilon = -\epsilon k(r(u^\epsilon) - w^\epsilon) \ \text{ on } \ \Gamma_{ij}(t),$$

where k is the Damköhler number, r is a rate function for the precipitation rate, and $w^\epsilon \in H(\text{dist}(x, B^\epsilon))$, with $B^\epsilon := \cup B_{ij}$, is a multivalued dissolution rate, with dist the Euclidean distance function, and with H the set-valued Heaviside graph:

$$H(u) = \begin{cases} \{0\} & \text{if} \quad u < 0, \\ [0,1] & \text{if} \quad u = 0, \\ \{1\} & \text{if} \quad u > 0. \end{cases}$$
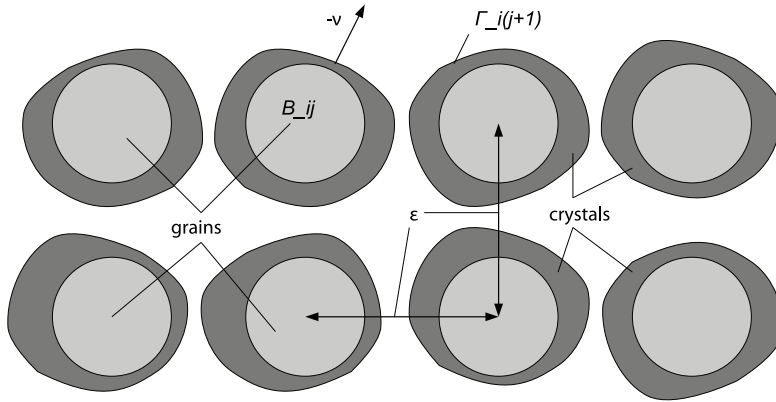
FIG. 1. *Schematic representation of a porous medium with layers of crystalline solid attached to the grains.*

In principle (2.1) determines the evolution and thus the position of the free interfaces $\Gamma_{ij}(t)$. To apply formal homogenization, we can, of course, expand the unknowns in (2.1) in a power series in ϵ, but it would be convenient not only to be able to expand the velocity of the interface but also to be able to expand the *position* of the interface in a power series in ϵ. The idea that we pursue in the present paper is to describe the free boundaries $\Gamma_{ij}(t)$ with a level set function. A level set function is a convenient tool for dealing with moving interfaces and has also inspired new ways of numerically solving moving boundary problems [9, 10, 11]. We identify the interface with the zero level set of the level set function, say S^ϵ. The level set equation

$$S_t^\epsilon + v_n^\epsilon |\nabla S^\epsilon| = 0$$

describes the evolution of the interface. We can now also expand the function S in a series and use the machinery of formal homogenization.

It is important to note that we assume that the layers of crystalline solid surrounding the different grains do not touch each other, so that $\Gamma_{ij}(t) \cap \Gamma_{kl}(t) = \emptyset$ if $i \neq k$ or $j \neq l$, and we also assume that the grains do not intersect the outer boundary of the domain Ω, so that $\Gamma \cap \Gamma_{ij}(t) = \emptyset$ for all i, j. We denote the solute concentration by u^ϵ, the velocity of the fluid phase by q^ϵ, and the pressure by p^ϵ. All of these unknowns are dimensionless. Note that for the formulation of the equations we need a continuous extension of u^ϵ to the whole of Ω, which is in equations below denoted by $\bar{u}^\epsilon$. The model is given by

$$(2.2) \quad \begin{cases} u_t^\epsilon = \nabla \cdot (D\nabla u^\epsilon - q^\epsilon u^\epsilon), \\ \epsilon^2 \mu \Delta q^\epsilon = \nabla p^\epsilon, \\ \nabla \cdot q^\epsilon = 0 \end{cases} \quad \text{in } \Omega^\epsilon(t),$$

$$(2.3) \quad \begin{cases} S_t^\epsilon = \epsilon k(r(\bar{u}^\epsilon) - w^\epsilon)|\nabla S^\epsilon|, \\ w^\epsilon \in H(\text{dist}(x, B^\epsilon)) \end{cases} \quad \text{in } \Omega,$$

$$(2.4) \quad \begin{cases} \nu^\epsilon \cdot (D\nabla u^\epsilon - q^\epsilon u^\epsilon) = -\epsilon k(r(u^\epsilon) - w^\epsilon)(\rho - u^\epsilon), \\ q^\epsilon = -\epsilon K k(r(u^\epsilon) - w^\epsilon)\nu^\epsilon \end{cases} \quad \text{on } \Gamma^\epsilon(t),$$

(2.5)
$$\begin{cases} u^\epsilon(x,t) = u_b(x,t), \\ q^\epsilon(x,t) = q_b(x,t) \end{cases} \quad \text{on } \Gamma,$$

(2.6)
$$\begin{cases} \bar{u}^\epsilon(x,0) = u_I(x), \\ S^\epsilon(x,0) = S_I(x) \end{cases} \quad \text{in } \Omega,$$

where

(2.7)
$$\Omega^\epsilon(t) := \{x \in \Omega \,|\, S^\epsilon(x,t) < 0\},$$

(2.8)
$$\Gamma^\epsilon(t) := \{x \in \Omega \,|\, S^\epsilon(x,t) = 0\},$$

and where

(2.9)
$$\nu^\epsilon = \frac{\nabla S^\epsilon}{|\nabla S^\epsilon|}$$

denotes the normal on the boundary $\Gamma^\epsilon(t)$.

The model equations contain the positive parameters D, the dimensionless diffusion coefficient, μ, the dimensionless viscosity, k, the Damköhler number, and ρ, the dimensionless density of the crystalline phase.

The auxiliary function w^ϵ acts as the scaled dissolution rate, and, when $\text{dist}(x, B^\epsilon) > 0$, w^ϵ attains the value 1, and when $\text{dist}(x, B^\epsilon) = 0$, we have $w^\epsilon = r(u^\epsilon)$. With respect to the reaction rate function $r(u)$, we assume the following:

1. $r : \mathbb{R} \to [0, \infty)$ is locally Lipschitz.
2. A unique $u_- \in [0, \rho)$ exists such that $r(u) = 0$ for all $u \le u_-$ and $r(u)$ is strictly increasing if $u > u_-$.
3. A unique $u_s \in (u_-, \rho)$ exists such that $r(u_s) = 1$.

The parameter K, which expresses volume changes due to precipitation or dissolution [17], may also be negative and is between the bounds

(2.10)
$$\frac{u_s - \rho}{u_s} < K < 1.$$

Furthermore, for the initial datum u_I we assume the following inequalities:

$$0 \le u_I < \rho \quad \text{in } \Omega.$$

3. Formal homogenization. In addition to the macroscopic variable x, we introduce a periodic unit cube with microscopic variable y ($y = (y_1, y_2)$, with $0 \le y_i \le 1$ for $i = 1, 2$). We assume that all of the unknowns are functions of x and y, such that

$$u^\epsilon = u^\epsilon(x, y, t), \quad S^\epsilon = S^\epsilon(x, y, t), \quad q^\epsilon = q^\epsilon(x, y, t), \quad p^\epsilon = p^\epsilon(x, y, t),$$

with $y = \frac{x}{\epsilon}$, where x captures the "slow" variations on the macroscopic scale and y the "fast" variations on the pore scale. For the formal homogenization we assume the following formal asymptotic expansions for u^ϵ, S^ϵ, q^ϵ, and p^ϵ:

$$u^\epsilon(x,t) = u_0(x, x/\epsilon, t) + \epsilon u_1(x, x/\epsilon, t) + \epsilon^2 u_2(x, x/\epsilon, t) + \cdots,$$
$$S^\epsilon(x,t) = S_0(x, x/\epsilon, t) + \epsilon S_1(x, x/\epsilon, t) + \epsilon^2 S_2(x, x/\epsilon, t) + \cdots,$$
$$q^\epsilon(x,t) = q_0(x, x/\epsilon, t) + \epsilon q_1(x, x/\epsilon, t) + \epsilon^2 q_2(x, x/\epsilon, t) + \cdots,$$
$$p^\epsilon(x,t) = p_0(x, x/\epsilon, t) + \epsilon p_1(x, x/\epsilon, t) + \epsilon^2 p_2(x, x/\epsilon, t) + \cdots,$$

where $u_k(\cdot, y, \cdot)$, $S_k(\cdot, y, \cdot)$, $q_k(\cdot, y, \cdot)$, and $p_k(\cdot, y, \cdot)$ are 1-periodic in $y = \frac{x}{\epsilon}$. The gradient of a function $f(x, \frac{x}{\epsilon})$, depending on x and $y = \frac{x}{\epsilon}$, is given by

$$\nabla f = \nabla_x f + \frac{1}{\epsilon}\nabla_y f|_{y=\frac{x}{\epsilon}}, \tag{3.1}$$

where ∇_x and ∇_y denote the gradients with respect to the first and second variables of f.

3.1. Preliminaries. In order to use formal homogenization, we first expand ν^ϵ in a power series in ϵ. This can be done in terms of S_i's using (2.9). We expand $|\nabla S^\epsilon|$: Using the chain rule (3.1) (see also [5]), the expansion for S^ϵ, and the Taylor series for the square root, we obtain

$$|\nabla S^\epsilon| = \frac{1}{\epsilon}|\nabla_y S_0| + (\cdots). \tag{3.2}$$

In the same fashion, we obtain

$$\nu^\epsilon = \nu_0 + \epsilon\nu_1 + \epsilon^2(\cdots),$$

where

$$\nu_0 = \frac{\nabla_y S_0}{|\nabla_y S_0|}$$

and

$$\nu_1 = \frac{\nabla_x S_0 + \nabla_y S_1}{|\nabla_y S_0|} - \frac{(\nabla_x S_0 \cdot \nabla_y S_0 + \nabla_y S_0 \cdot \nabla_y S_1)}{|\nabla_y S_0|^2}\frac{\nabla_y S_0}{|\nabla_y S_0|}.$$

If we introduce the normalized tangential vector τ_0, with $\tau_0 \perp \nu_0$, then we can write

$$\nu_1 = \tau_0\frac{\tau_0 \cdot (\nabla_x S_0 + \nabla_y S_1)}{|\nabla_y S_0|}. \tag{3.3}$$

Now we focus on the boundary conditions at the moving boundary $\Gamma^\epsilon(x, t)$. In order to obtain boundary conditions, we need to substitute the expansions for u^ϵ, q^ϵ, and ν^ϵ into the boundary conditions (2.4). This is not so straightforward as it may seem, since the boundary conditions (2.4) are enforced at $\Gamma^\epsilon(t)$, i.e., at every x where $S^\epsilon(x, t) = 0$. For the formulation of the upscaled model it would be convenient to have a boundary condition enforced at $\Gamma_0(x, t) := \{y \mid S_0(x, y, t) = 0\}$. To obtain such an equation, we suppose that we can parametrize the part of the boundary $\Gamma^\epsilon_{ij}(t)$ that surrounds the sphere B_{ij} with $k^\epsilon(s, t)$, so that it holds that

$$S^\epsilon(k^\epsilon(s, t), t) = 0 \quad \text{for all } t \geq 0,$$

and we assume that we can expand $k^\epsilon(s, t)$ using the formal asymptotic expansion

$$k^\epsilon(s, t) = x + \epsilon k_0(s, t) + \epsilon^2 k_1(s, t) + \epsilon^3(\cdots), \tag{3.4}$$

with $x = (\epsilon i, \epsilon j)$. Using the expansion for S^ϵ, the periodicity of S_i in y, and the Taylor series for S_0 and S_1 around (x, k_0), we obtain

$$S_0(x, k_0, t) + \epsilon(S_1(x, k_0, t) + k_0 \cdot \nabla_x S_0(x, k_0, t) + k_1 \cdot \nabla_y S_0(x, k_0, t)) + \epsilon^2(\cdots) = 0.$$

Collecting terms with the same order of ϵ, we see that $k_0(s,t)$ parametrizes locally the zero level set of S_0:

$$S_0(x, k_0, t) = 0.$$

For k_1, we have the equation

(3.5) $$S_1(x, k_0, t) + k_0 \cdot \nabla_x S_0(x, k_0, t) + k_1 \cdot \nabla_y S_0(x, k_0, t) = 0.$$

It suffices to search for k_1 that is aligned with ν_0, so that we write

(3.6) $$k_1(s,t) = \lambda(s,t)\nu_0(s,t) = \lambda\frac{\nabla_y S_0}{|\nabla_y S_0|},$$

where, using (3.5), λ is given by

(3.7) $$\lambda = -\frac{S_1}{|\nabla_y S_0|} - \frac{k_0 \cdot \nabla_x S_0}{|\nabla_y S_0|}.$$

Let us consider an abstract boundary condition that can be written in the form

$$K(x, x/\epsilon, t) = 0 \quad \text{for } x \in \Gamma^\epsilon(t).$$

Using the expansion (3.4) and the Taylor series for K around (x, k_0), we obtain

(3.8)
$$K(x, k_0, t) + \epsilon(k_0 \cdot \nabla_x K(x, k_0, t) + k_1 \cdot \nabla_y K(x, k_0, t))$$
$$+ \frac{\epsilon^2}{2}(k_0, k_1) \cdot (\mathcal{D}^2 K(x, k_0, t))(k_0, k_1) + \epsilon^3(\cdots) = 0,$$

where $\mathcal{D}^2 K$ denotes the Hessian of K, with respect to x and y. Substituting the expression (3.6), we can restate (3.8) in the following way:

(3.9)
$$K(x, y, t) + \epsilon(y \cdot \nabla_x K(x, y, t) + \lambda\nu_0 \cdot \nabla_y K(x, y, t))$$
$$+ \frac{\epsilon^2}{2}(y, \lambda\nu_0) \cdot (\mathcal{D}^2 K(x, y, t))(y, \lambda\nu_0) + \epsilon^3(\cdots) = 0 \quad \text{for } y \in \Gamma_0(x, t).$$

Furthermore, we will need the following technical lemmas in the subsequent sections.

LEMMA 3.1. *Let $g(x, y, t)$ be a scalar function such that $g(x, y, t) = 0$ for $y \in \Gamma_0(x, t)$, $x \in \Omega$, and $t \geq 0$; then it holds that*

$$\nabla_x g = \frac{\nu_0 \cdot \nabla_y g}{|\nabla_y S_0|}\nabla_x S_0 \quad \text{for } x \in \Omega,\ t \geq 0,\ y \in \Gamma_0(x, t).$$

Proof. Let $k_0(s, x)$ for $0 \leq s \leq 1$ parametrize $\Gamma_0(x, t)$. This means $S_0(x, k_0(s, x)) = 0$, and since $g = 0$ on $\Gamma_0(x, t)$, we also have $g(x, k_0(s, x)) = 0$. By differentiation with respect to x_i, for $i = 1, 2$, we obtain

$$\partial_{x_i} S_0 = -\nabla_y S_0 \cdot \partial_{x_i} k_0 = -|\nabla_y S_0|\nu_0 \cdot \partial_{x_i} k_0,$$
$$\partial_{x_i} g = -\nabla_y g \cdot \partial_{x_i} k_0 = -|\nabla_y S_0|\nu_0 \cdot \partial_{x_i} k_0.$$

Since g is zero on Γ_0, its gradient is parallel to ν_0 and thus $\nabla_y g = (\nu_0 \cdot \nabla_y g)\nu_0$, so that we obtain

$$\partial_{x_i} g = -\nabla_y g \cdot \partial_{x_i} k_0 = -(\nu_0 \cdot \nabla_y g)(\nu_0 \cdot \partial_{x_i} k_0) = \frac{\nu_0 \cdot \nabla_y g}{|\nabla_y S_0|}\partial_{x_i} S_0.$$

This proves the lemma.   ☐

LEMMA 3.2. *Let $F(x,y,t)$ be a vector-valued function such that $\nabla_y \cdot F(x,y,t) = 0$ on $Y_0(x,t) := \{y \mid S_0(x,y,t) < 0\}$ and $\nu_0 \cdot F(x,y,t) = 0$ on $\Gamma_0(x,t)$ for $x \in \Omega$ and $t \geq 0$. Then it holds that*

$$\int_{\Gamma^0(x,t)} \frac{\tau_0 \cdot \nabla_y S_1}{|\nabla_y S_0|} \tau_0 \cdot F - \frac{S_1}{|\nabla_y S_0|} \nu_0 \cdot \nabla_y(\nu^0 \cdot F) \, d\sigma = 0 \quad \text{for } x \in \Omega, \ t \geq 0.$$

Proof. We study variations of the integral

$$(3.10) \qquad\qquad I_\delta = \int_{Y^\delta(x,t)} \nabla_y \cdot F(x,y,t) \, dy$$

with respect to variation of the domain of integration. Here $Y^\delta(x,t)$ is the region where $S_0(x,y,t) + \delta S_1(x,y,t) < 0$. In order to make sure that Y^δ is included in Y_0 on which F is defined, we split S_1 into its positive and negative parts, $S_1 = [S_1]_+ - [S_1]_-$, and define $Y_+^\delta := \{y \mid S_0 + \delta[S_1]_+ < 0\}$ and $Y_-^\delta := \{y \mid S_0 + \delta[S_1]_- < 0\}$ which are both, for positive δ, contained in Y_0. The right derivative with respect to δ of the integrals

$$\int_{Y_+^\delta} \nabla_y \cdot F(x,y,t) \, dy \quad \text{and} \quad \int_{Y_-^\delta} \nabla_y \cdot F(x,y,t) \, dy$$

equals zero due to the fact that $\nabla_y \cdot F = 0$ on $Y_0(x,t)$. Now suppose that $k_+(s,\delta)$ parametrizes $\Gamma_+^\delta := \partial Y_+^\delta$ so that $S_0(x,k_+(s,\delta),t) + \delta[S_1]_+(x,k_+(s,\delta),t) = 0$. By differentiation with respect to δ we obtain

$$(3.11) \qquad \nabla_y S_0 \partial_\delta k_+ + [S_1]_+ + \delta \nabla_y [S_1]_+ \partial_\delta k_+ = 0 \quad \text{for } y \in \Gamma_+^\delta.$$

Thus for $\delta = 0$, we have $\nabla_y S_0 \partial_\delta k_+ = -[S_1]_+$. Now we compute, where all derivatives with respect to δ are right derivatives,

$$0 = \partial_\delta \int_{Y_+^\delta} \nabla_y \cdot F \, dy|_{\delta=0} = \partial_\delta \int_{\Gamma_+^\delta} \nu^\delta \cdot F \, d\sigma|_{\delta=0}$$

$$= \partial_\delta \int_0^1 \nu^\delta \cdot F(x, k_+(s,\delta), t) |\partial_s k_+(s,\delta)| \, ds|_{\delta=0}$$

$$= \int_0^1 \left(\partial_\delta \nu^\delta|_{\delta=0} \cdot F + \nabla_y(\nu^0 \cdot F) \cdot \partial_\delta k_+|_{\delta=0} \right) |\partial_s k_+(s,0)| \, ds$$

$$+ \int_0^1 \nu^0 \cdot F \partial_\delta(|\partial_s k_+(s,\delta)|)|_{\delta=0} \, ds$$

$$= \int_{\Gamma^0} \frac{\tau_0 \cdot \nabla_y [S_1]_+}{|\nabla_y S_0|} \tau_0 \cdot F - \frac{[S_1]_+}{|\nabla_y S_0|} \nu_0 \cdot \nabla_y(\nu^0 \cdot F) \, d\sigma.$$

For the last equality, we again use that $\nu^0 \cdot F = 0$ on Γ^0 so that $\nabla_y(\nu^0 \cdot F) = (\nu_0 \cdot \nabla_y(\nu_0 \cdot F))\nu_0$. We also use a formula similar to (3.3) for the derivative of ν^δ with respect to δ. For the remainder of the proof, we also perform the above computation for the negative part $[S_1]_-$ and then subtract the results to complete the proof.   ☐

3.2. Level set equation. Before we proceed with the substitution of the formal expansions into the model equations, we will first regularize the set-valued Heaviside

graph. This means that we replace H in (2.3_2) with H_δ which is defined, for small $\delta > 0$, by

$$(3.12) \qquad H_\delta(d) := \begin{cases} 0 & \text{if } d < 0, \\ d/\delta & \text{if } d \in [0, \delta], \\ 1 & \text{if } d > \delta. \end{cases}$$

Furthermore, we introduce the notation

$$f_\delta(u^\epsilon, y) := k\big(r(u^\epsilon) - H_\delta(\text{dist}(\epsilon y, B^\epsilon))\big),$$

where $f_\delta(\cdot, y)$ is 1-periodic in y. We replace (2.3) and (2.4) with

$$S_t^\epsilon = \epsilon f_\delta(u^\epsilon, x/\epsilon)|\nabla S^\epsilon| \quad \text{in } \Omega,$$

$$\begin{cases} \nu^\epsilon \cdot (D\nabla u^\epsilon - q^\epsilon u^\epsilon) = -\epsilon f_\delta(u^\epsilon, x/\epsilon)(\rho - u^\epsilon), \\ q^\epsilon = -\epsilon K f_\delta(u^\epsilon, x/\epsilon)\nu^\epsilon \end{cases} \quad \text{on } \Gamma^\epsilon(t).$$

Since r and H_δ are both Lipschitz, we now write

$$f_\delta(u^\epsilon, y) = f_\delta(u_0, y) + \epsilon(\cdots).$$

Substituting (3.2) into (2.3_1) and using the above expression, we obtain the equation

$$\partial_t S_0 - f_\delta(u_0, y)|\nabla_y S_0| + \epsilon(\cdots) = 0.$$

Keeping only terms independent of ϵ and letting $\delta \to 0$, we obtain (using similar arguments as in, e.g., [15, Theorem 2.21])

$$(3.13) \qquad \partial_t S_0 = f(u_0, y)|\nabla_y S_0|,$$

where $f(u_0, y) = k(r(u_0) - w)$, with $w \in H(\text{dist}(\epsilon y, B^\epsilon))$. Note that this last expression does not depend on ϵ.

3.3. Convection-diffusion equation. When we substitute the asymptotic expansion for u^ϵ into (2.2_1), we obtain

$$(3.14) \quad \begin{aligned} \partial_t u_0 = {} & \frac{1}{\epsilon^2} D\Delta_y u_0 + \frac{1}{\epsilon}(\nabla_y \cdot F + \nabla_x \cdot (D\nabla_y u_0)) \\ & + \nabla_y \cdot (D(\nabla_y u_2 + \nabla_x u_1) - q_1 u_0 - q_0 u_1) + \nabla_x \cdot F \\ & + \epsilon(\cdots), \end{aligned}$$

where $F = D(\nabla_x u_0 + \nabla_y u_1) - q_0 u_0$. Now we will first expand (2.4_1), using the expansions for u^ϵ, ν^ϵ and the Taylor series of f around u_0:

$$\begin{aligned} 0 = {} & \nu^\epsilon \cdot (D\nabla u^\epsilon - q^\epsilon u^\epsilon) - f(u^\epsilon, y)(\rho - u^\epsilon) \\ = {} & \frac{1}{\epsilon}\nu_0 \cdot (D\nabla_y u_0) + \nu_0 \cdot F + \nu_1 \cdot (D\nabla_y u_0) \\ & + \epsilon\Big(\nu_0 \cdot (D(\nabla_x u_1 + \nabla_y u_2) - q_1 u_0 - q_0 u_1) + \nu_1 \cdot F + \nu_2 \cdot (D\nabla_y u_0) - f(u_0, y)(\rho - u_0)\Big) \\ & + \epsilon^2(\cdots) \quad \text{for } x \in \Gamma^\epsilon(t), \ y = \frac{x}{\epsilon}, \end{aligned}$$

and next we substitute this expansion into (3.9) and thus obtain

$$
\begin{aligned}
0 = &\frac{1}{\epsilon}\nu_0 \cdot (D\nabla_y u_0) \\
&+ \nu_0 \cdot F + \nu_1 \cdot (D\nabla_y u_0) + y \cdot \nabla_x(\nu_0 \cdot (D\nabla_y u_0)) + \lambda\nu_0 \cdot \nabla_y(\nu_0 \cdot (D\nabla_y u_0)) \\
&+ \epsilon\Big(\nu_0 \cdot (D(\nabla_x u_1 + \nabla_y u_2) - q_1 u_0 - q_0 u_1) + \nu_1 \cdot F + \nu_2 \cdot (D\nabla_y u_0) \\
&\quad - f(u_0)(\rho - u_0) + y \cdot \nabla_x(\nu_0 \cdot F + \nu_1 \cdot (D\nabla_y u_0)) + \lambda\nu_0 \cdot \nabla_y(\nu_0 \cdot F \\
&\quad + \nu_1 \cdot (D\nabla_y u_0)) + \frac{1}{2}(y, \lambda\nu_0) \cdot (\mathcal{D}^2(\nu_0 \cdot (D\nabla_y u_0)))(y, \lambda\nu_0)\Big) \\
&+ \epsilon^2(\cdots) \quad \text{for } y \in \Gamma_0(x, t).
\end{aligned}
$$

(3.15)

Now we collect the ϵ^{-2}-term from (3.14) and the ϵ^{-1}-term from (3.15) and obtain for u_0 the equations

(3.16)
$$
\begin{cases}
\Delta_y u_0 = 0 & \text{in } Y_0(x, t), \\
\nu_0 \cdot \nabla_y u_0 = 0 & \text{on } \Gamma_0(x, t), \\
\text{periodicity in } y,
\end{cases}
$$

where $Y_0(x, t) = \{y \mid S_0(x, y, t) < 0\}$. This means that u_0 is determined up to a constant and does not depend on y, so that $\nabla_y u_0 = 0$. Collecting the ϵ^{-1}-terms from (3.14), the ϵ^0-terms from (3.15), and using that $\nabla_y u_0 = 0$, we get for u_1 the equations

(3.17)
$$
\begin{cases}
\nabla_y \cdot (D\nabla_y u_1 - q_0 u_0) = 0 & \text{in } Y_0(x, t), \\
\nu_0 \cdot (D(\nabla_x u_0 + \nabla_y u_1) - q_0 u_0) = 0 & \text{on } \Gamma_0(x, t), \\
\text{periodicity in } y.
\end{cases}
$$

Next we collect the ϵ^0-terms from (3.14) and the ϵ^1-terms from (3.15) and obtain

(3.18)
$$
\begin{cases}
\partial_t u_0 = \nabla_y \cdot (D(\nabla_y u_2 + \nabla_x u_1) - q_1 u_0 - q_0 u_1) + \nabla_x \cdot F & \text{in } Y_0(x, t), \\
\nu_0 \cdot (D(\nabla_x u_1 + \nabla_y u_2) - q_1 u_0 - q_0 u_1) = -\nu_1 \cdot F \\
\quad + f(u_0)(\rho - u_0) - y \cdot \nabla_x(\nu_0 \cdot F) - \lambda\nu_0 \cdot \nabla_y(\nu_0 \cdot F) & \text{on } \Gamma_0(x, t), \\
\text{periodicity in } y.
\end{cases}
$$

Integrating (3.18_1) over $Y_0(x, t)$ and using the boundary condition (3.18_2) gives

$$
\begin{aligned}
|Y_0(x, t)|\partial_t u_0 = &\int_{Y_0(x,t)} \nabla_y \cdot (D(\nabla_x u_1 + \nabla_y u_2) - q_1 u_0 - q_0 u_1)\, dy + \int_{Y_0(x,t)} \nabla_x \cdot F\, dy \\
= &\int_{\Gamma_0(x,t)} -\nu_1 \cdot F + f(u_0)(\rho - u_0) - y \cdot \nabla_x(\nu_0 \cdot F) - \lambda\nu_0 \cdot \nabla_y(\nu_0 \cdot F)\, d\sigma \\
&+ \nabla_x \cdot \int_{Y_0(x,t)} F\, dy + \int_{\Gamma_0(x,t)} \frac{\nabla_x S_0}{|\nabla_y S_0|} \cdot F\, d\sigma.
\end{aligned}
$$

This can be rewritten, using (3.3) and the boundary condition from (3.17), as

$$
\partial_t(|Y_0(x, t)|u_0) = \nabla_x \cdot \int_{Y_0(x,t)} (D(\nabla_y u_1 + \nabla_x u_0) - q_0 u_0)\, dy + |\Gamma_0(x, t)|f(u_0)\rho - I_1 - I_2,
$$

where

$$I_1 = \int_{\Gamma_0(x,t)} y \cdot \nabla_x g - \frac{y \cdot \nabla_x S_0}{|\nabla_y S_0|} \nu_0 \cdot \nabla_y g \, d\sigma,$$

$$I_2 = \int_{\Gamma_0(x,t)} \frac{\tau_0 \cdot \nabla_y S_1}{|\nabla_y S_0|} \tau_0 \cdot F - \frac{S_1}{|\nabla_y S_0|} \nu_0 \cdot \nabla_y (\nu^0 \cdot F) \, d\sigma,$$

with $g = \nu_0 \cdot F$, and where we have used (3.7). The boundary condition (3.17$_2$) gives us $g(x, y, t) = 0$ for $y \in \Gamma_0(x, t)$, and now we invoke Lemma 3.1 to obtain $\nabla_x g = \frac{\nu_0 \cdot \nabla_y g}{|\nabla_y S_0|} \nabla_x S_0$, so that $I_1 = 0$. For the integral I_2 we invoke Lemma 3.2 to obtain $I_2 = 0$.

3.4. Stokes equation. Substituting the asymptotic expansions for q^ϵ and p^ϵ into (2.2$_{2,3}$), we obtain

(3.19) $$\mu \Delta_y q_0 = \frac{1}{\epsilon} \nabla_y p_0 + \nabla_y p_1 + \nabla_x p_0 + \epsilon(\cdots),$$

(3.20) $$\frac{1}{\epsilon} \nabla_y \cdot q_0 + \nabla_x \cdot q_0 + \nabla_y \cdot q_1 + \epsilon(\cdots) = 0,$$

and substituting the expansion into the boundary condition (2.4$_2$), and using (3.9), gives

(3.21) $$q_0 + \epsilon \Big(q_1 - K f(u_0) \nu_0 + (\nabla_x q_0)^T y + \lambda (\nabla_y q_0)^T \nu_0 \Big) + \epsilon^2(\cdots) = 0 \quad \text{for } y \in \Gamma_0(x, t).$$

The ϵ^{-1}-term in (3.19) states that $\nabla_y p_0 = 0$, so that we conclude that p_0 is independent of y. Furthermore, we obtain, after collecting ϵ^0-terms from (3.19) and (3.21) and ϵ^{-1}-terms from (3.20), the equations for q_0 and p_1:

(3.22) $$\begin{cases} \mu \Delta_y q_0 = \nabla_y p_1 + \nabla_x p_0 & \text{in } Y_0(x, t), \\ \nabla_y \cdot q_0 = 0 & \text{in } Y_0(x, t), \\ q_0 = 0 & \text{on } \Gamma_0(x, t), \\ \text{periodicity in } y. \end{cases}$$

These equations determine the averaged velocity field given by

$$\bar{q}(x, t) = \int_{Y_0(x,t)} q_0(x, y, t) \, dy.$$

Now we compute the divergence of $\bar{q}$ (where we use the ϵ^0-terms from (3.20)):

$$\nabla_x \cdot \bar{q} = \nabla_x \cdot \int_{Y_0(x,t)} q_0 \, dy = \int_{Y_0(x,t)} \nabla_x \cdot q_0 \, dy - \int_{\Gamma_0(x,t)} \frac{\nabla_x S_0}{|\nabla_y S_0|} \cdot q_0 \, d\sigma$$

$$= -\int_{Y(x,t)} \nabla_y \cdot q_1 \, dy = -\int_{\Gamma_0(x,t)} \nu_0 \cdot q_1 \, d\sigma$$

$$= \int_{\Gamma_0(x,t)} K f(u_0) - \nu_0 \cdot ((\nabla_x q_0)^T y + \lambda (\nabla_y q_0)^T \nu_0) \, d\sigma$$

$$= |\Gamma_0(x, t)| K f(u_0) - I_1 - I_2,$$

with

$$I_1 = \int_{\Gamma_0(x,t)} \nu_0 \cdot \left((\nabla_x q_0)^T y - \frac{y \cdot \nabla_x S_0}{|\nabla_y S_0|} (\nabla_y q_0)^T \nu_0 \right) d\sigma,$$

$$I_2 = - \int_{\Gamma_0(x,t)} \nu_0 \cdot \left(\frac{S_1}{|\nabla_y S_0|} (\nabla_y q_0)^T \nu_0 \right) d\sigma.$$

We apply Lemma 3.1 to $g = \nu_0 \cdot q_0$, and we obtain

$$\nabla_x(\nu_0 \cdot q_0) = \frac{\nu_0 \cdot \nabla_y(\nu_0 \cdot q_0)}{|\nabla_y S_0|} \nabla_x S_0 \quad \text{on } \Gamma_0(x,t).$$

Since $q_0 = 0$ on $\Gamma_0(x,t)$, it follows that $(\nabla_x q_0)^T \nu_0 = \frac{\nu_0 \cdot (\nabla_y q_0)^T \nu_0}{|\nabla_y S_0|} \nabla_x S_0$, so that $I_1 = 0$. Next we apply Lemma 3.2 to q_0, and consequently

$$\int_{\Gamma^0} \frac{\tau_0 \cdot \nabla_y S_1}{|\nabla_y S_0|} \tau_0 \cdot q_0 - \frac{S_1}{|\nabla_y S_0|} \nu_0 \cdot \nabla_y(\nu^0 \cdot q_0) \, d\sigma = 0,$$

and again using $q_0 = 0$ on $\Gamma_0(x,t)$, it follows that $I_2 = 0$.

4. Upscaled equations and simplification. As usual, we write the solutions of (3.17) and (3.22) in terms of the solutions of the following two cell problems [5]:

$$(4.1) \qquad \begin{cases} \Delta_y v_j = 0 & \text{in } Y_0(x,t), \\ \nu_0 \nabla_y v_j = -e_j & \text{on } \Gamma_0(x,t), \\ \text{periodicity in } y \end{cases}$$

and

$$(4.2) \qquad \begin{cases} \Delta_y w_j = \nabla_y \pi_j + e_j & \text{in } Y_0(x,t), \\ \nabla_y \cdot w_j = 0 & \text{in } Y_0(x,t), \\ w_j = 0 & \text{on } \Gamma_0(x,t), \\ \text{periodicity in } y \end{cases}$$

for $j = 1, 2$. This allows us to write the results of the formal homogenization procedure in the form of the following distributed microstructure model [5]:

$$(4.3) \qquad \begin{cases} \partial_t S_0(x,y,t) + f(u_0(x,t),y)|\nabla_y S_0(x,y,t)| = 0 & \text{for } y \in [0,1]^2, \ x \in \Omega, \\ \partial_t(|Y_0(x,t)|u_0) = \nabla_x \cdot (D\mathcal{A}(x,t)\nabla_x u_0 - \bar{q}u_0) + |\Gamma_0(x,t)|f(u_0)\rho & \text{for } x \in \Omega, \\ \bar{q} = -\frac{1}{\mu}\mathcal{K}(x,t)\nabla_x p_0 & \text{for } x \in \Omega, \\ \nabla_x \cdot \bar{q} = |\Gamma_0(x,t)|Kf(u_0) & \text{for } x \in \Omega, \end{cases}$$

$$(4.4) \qquad \begin{cases} u_0(x,t) = u_b(x,t) & \text{for } x \in \Gamma, \\ \bar{q}(x,t) = q_b(x,t) & \text{for } x \in \Gamma, \end{cases}$$

$$(4.5) \qquad \begin{cases} u_0(x,0) = u_I(x), \\ S_0(x,y,0) = S_I(x,y), \end{cases}$$

where the tensors $\mathcal{A}(x,t) = (a_{ij})_{i,j}$ and $\mathcal{K}(x,t) = (k_{ij})_{i,j}$ are given by

$$a_{ij} = \int_{Y_0(x,t)} \delta_{ij} + \partial_{y_i} v_j \, dy$$

and

$$k_{ij} = \int_{Y_0(x,t)} w_{ji} \, dy.$$

For computational purposes, the distributed microstructure model as introduced above is more preferable than the original microscale model: It does not depend on ϵ, and thus the numerical discretization does not need to become finer and finer for smaller ϵ, which is the case for the original microscale model. However, it is still computationally expensive since it involves solving two cell problems for each x-gridpoint. This can be drastically reduced if we assume special initial microscale geometries. If we start with spherical grain boundaries, i.e., if the sets $\Gamma_0(x,0) = \{y \mid S_0(x,y,0) = 0\}$ are a circle, then, since $f(u_0(x,t), y)$ is spherically symmetric in y for each $x \in \Omega$, solutions of the level set equation (4.3_1) will be such that the sets $\Gamma_0(x,t)$ will stay a circle for all $x \in \Omega$ and $t > 0$. This means that in this case the equation (4.3_1) can be reduced to

(4.6) $\qquad \partial_t R(x,t) = f(u_0(x,t), R(x,t)) = k(r(u_0(x,t)) - w(x,t)),$

with $w \in H(R(x,t) - R_{\min})$, and where $R(x,t)$ denotes the radius of $\Gamma_0(x,t)$. The other equations in (4.3) can also be simplified, and we obtain the system

$$(4.7) \quad \begin{cases} \partial_t R = k(r(u_0) - w), \\ w \in H(R - R_{\min}), \\ \partial_t((1 - \pi R^2)u_0) = \nabla_x \cdot (D\mathcal{A}(R)\nabla_x u_0 - \bar{q}u_0) + 2\pi Rk(r(u_0) - w)\rho, \qquad \text{in } \Omega, \\ \bar{q} = -\frac{1}{\mu}\mathcal{K}(R)\nabla_x p_0, \\ \nabla_x \cdot \bar{q} = 2\pi RKk(r(u_0) - w) \end{cases}$$

$$(4.8) \quad \begin{cases} u_0(x,t) = u_b(x,t), \\ \bar{q}(x,t) = q_b(x,t) \end{cases} \qquad \text{on } \Gamma,$$

$$(4.9) \quad \begin{cases} u_0(x,0) = u_I(x), \\ R(x,0) = R_I(x) \end{cases}$$

where the tensors $\mathcal{A}(R(x,t))$ and $\mathcal{K}(R(x,t))$ are again determined by the solutions of the cell problems (4.1) and (4.2) which now depend only on $R(x,t)$, since $Y_0(x,t)$ is determined by $R(x,t)$. Note that the same reduction can also be obtained for different initial grain geometries: For ellipses the same would hold. The important condition is that solutions of the level set equation are in a certain sense shape invariant and can be parametrized with a single parameter.

5. Numerical experiments. In this section we compare numerical solutions of the original equations on the microscale with numerical solutions of the homogenized equations in order to see how well the homogenized equations approximate the averaged behavior of the original model. As a first test we compare the solution of the upscaled equations (4.7)–(4.9) to solutions of the original microscale model (2.2)–(2.6).
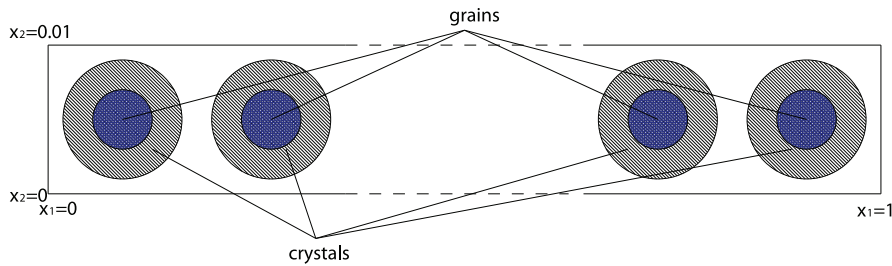
FIG. 2. *The initial configuration for the microscale numerical experiments.*

The initial configuration for the microscale model is shown in Figure 2: We consider a strip of length 1 and width 0.01 with a periodic array of inclusions. The inclusions are circles with initial radius 0.4, and with midpoints $(x, y) = (0.005 + 0.01k, 0.005)$, for $k = 0, 1, 2, \ldots, 99$, and consist of a grain of radius 0.2 and a layer of crystalline solid with thickness 0.2. Thus initially we have a square periodic cell with height and length $\epsilon = 0.01$. Furthermore, we consider periodicity in the "vertical" x_2-direction. This means that the domain Ω in the upscaled equations (4.7) reduces to the interval $(0, 1)$.

For the microscale equations (2.2)–(2.6) we use the following parameter values:

$$(5.1) \qquad \begin{array}{ccc} D = 1, & \mu = 1, & k = 1, \\ \rho = 2, & r(u) = u, & K = 0, \end{array}$$

and we use the following boundary conditions in (2.5):

$$(5.2) \qquad \begin{cases} u_b = 0, \\ q_b = \begin{pmatrix} 1 \\ 0 \end{pmatrix} \end{cases} \qquad \text{for } x_1 = 0,$$

$$(5.3) \qquad \begin{cases} \nu \cdot \nabla u = 0, \\ p^\epsilon I + \frac{\mu}{2}(\nabla q^\epsilon + (\nabla q^\epsilon)^T) = 0 \end{cases} \qquad \text{for } x_1 = 1,$$

$$(5.4) \qquad \text{periodicity in } x_2,$$

and for the initial conditions in (2.6) we use

$$u_I \equiv 1.$$

For the homogenized equations (4.7)–(4.9) this results in the same parameter values as in (5.1). The corresponding boundary conditions in (4.8) are

$$(5.5) \qquad \begin{cases} u_b = 0, \\ q_b = 1 \end{cases} \qquad \text{for } x = 0,$$

$$\partial_x u = 0 \quad \text{for } x = 1,$$

and the corresponding initial conditions in (4.9) are

$$u_I \equiv 1, \quad R_I \equiv 0.4.$$

Note that, since $K = 0$, we do not need to solve for $\bar{q}$. Due to (4.7_4) we have that $\bar{q} = q_b$ for all $x \in [0,1]$. Also note that for a one-dimensional setting such as the present one, we actually do not need to compute the effective permeability tensor $\mathcal{K}$ if we supply a boundary condition for $\bar{q}$. If we supply a pressure drop, then we do need to know the tensor $\mathcal{K}$, as we do for computations in a two-dimensional or higher-dimensional setting.

5.1. Microscale models: Arbitrary Lagrangian–Eulerian method. For the numerical solution of the microscale model we do not use the level set formulation, but we use the arbitrary Lagrangian–Eulerian (ALE) method [2], where we use normal velocity as given in (2.1) for the computation of the deformation of the ALE mesh. The ALE method has been developed to solve partial differential equations on moving domains. In this method the partial time derivatives are expressed with respect to a fixed reference configuration. A map, called the ALE map, $\chi_t : \Omega_0 \to \Omega(t)$, associates, at each time t, a point in the current computational domain $\Omega(t)$ with a point in the reference domain Ω_0. In this way, the system of ordinary differential equations resulting after space discretization describes the evolution of the solutions along trajectories that are at all times contained in the computational domain. We use the ALE method as implemented in the COMSOL Multiphysics package [1], with Laplacian smoothing [2]. For more details on the ALE method we refer the reader to [1, 2], and we also refer the reader to [17] for the application of the ALE method to crystal dissolution. We discretize (2.2)–(2.6) using 16261 quadratic elements, resulting in 218961 unknowns. Furthermore, we regularize the set-valued Heaviside graph H for the numerical computations: We replace it by H_δ so that in (2.1) for the normal velocity of the free boundary we have

$$w^\epsilon(x,t) = H_\delta(|(x_1 \,(\mathrm{mod}\, 0.01), x_2) - (0.005, 0.005)| - 0.002),$$

with H_δ as defined in (3.12) with $\delta = 0.01$.

5.2. Upscaled model: Effective diffusion and permeability tensors. In order to numerically approximate solutions of the upscaled equations (4.7), we need to compute the effective diffusion and permeability tensors as a function of the radius of the grain in the local cell problem. It is easily seen that in this case, due to symmetry, the tensors are in fact coefficients. We solved the cell problems (4.1) and (4.2) using a finite element discretization (quadratic elements) for various values of R. The values of R are taken on a equidistant grid on the interval $[0.2, 0.5]$ with 25 grid points. The number of finite elements ranged from 866 for $R = 0.2$ to 450 for $R = 0.4985$. In order to obtain a simple formula for the diffusion and permeability tensors as a function of R, we fitted these results with a fourth order polynomial in $(0.5 - R)^{1/2}$ for the diffusion coefficient and a third order polynomial in $(0.5 - R)$ for the permeability coefficient, which resulted in the following functions for $\mathcal{A}(R)$ and $\mathcal{K}(R)$:

$$\mathcal{A}(R) = 0.639879(0.5 - R)^{1/2} + 0.665634(0.5 - R) + 2.128861(0.5 - R)^{3/2}$$
$$-1.332304(0.5 - R)^2,$$
$$\mathcal{K}(R) = 0.000207(0.5 - R) + 0.090013(0.5 - R)^2 + 0.913720(0.5 - R)^3.$$

The choice for the form of these polynomials was based on the form of the graphs in Figure 3, where we have in both cases $\mathcal{A}(0.5) = 0$ and $\mathcal{K}(0.5) = 0$. (Note that we fitted these graphs only on the interval $[0.2, 0.5]$, since the grain radii equal 0.2 in the scaled cell problems.) With the fits given above, the maximal error in the computed
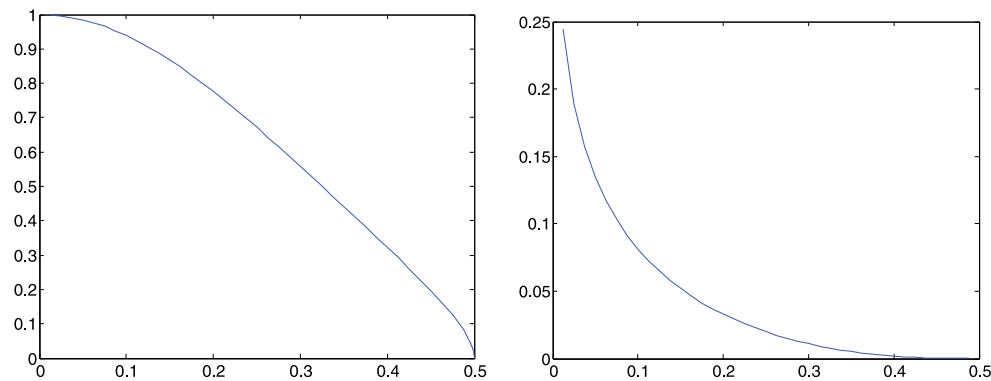
FIG. 3. *The effective diffusion coefficient (left plot) and the effective permeability coefficient (right plot) as a function of the radius of the grain.*

points was in the order of 10^{-3} for the diffusion coefficient and in the order of 10^{-4} for the permeability coefficient.

For the numerical solution of (4.7)–(4.9), we use a discretization of the interval $[0, 1]$ into 240 quadratic elements, which results in a system with 722 unknowns. Furthermore, for the homogenized equations we also regularize the set-valued Heaviside graph H so that in (4.7_2) we obtain

$$w(R) = H_\delta(R - 0.2),$$

with $\delta = 0.01$.

5.3. Numerical results: Microscale vs. upscaled equations. Initially, for $t = 0$, the system is in equilibrium: For the initial condition $u_I \equiv 1$ it holds that $r(u_I) = u_I = 1$ so that there is no dissolution or precipitation. For positive t there is, due to the boundary condition $u_b = 0$ for $x_1 = 0$ in (5.2) and for $x = 0$ in (5.5), transport of fluid with a low concentration of solute by diffusion and convection, and dissolution will start, first at the left end of the domain.

In Figure 4 the ALE mesh is shown. The top plot depicts a part of the mesh at the left part of the domain in its initial state. The bottom plot depicts the mesh after all of the crystalline solid is dissolved and the boundary of the mesh is located at the boundary of the grains.

In Figure 5 the profiles of solutions of the microscale model and the homogenized model are compared for two different time instants, $t = 0.05$ and $t = 0.5$. In the left plot the concentrations u^ϵ and u_0 are given. For the microscale model the concentration u^ϵ (represented by the dots) is plotted along the line $y = 0$. In the right plot the radius R is plotted for the homogenized equations and an estimate of the radius of the inclusions for the microscale equations (again represented by the dots). We see that for $t = 0.05$ only a small amount of crystalline solid is dissolved, while for $t = 0.5$ in approximately the left half of the domain all of the crystalline solid is already dissolved. We also see that the results for the microscale equations and the homogenized equations match very well.

6. Conclusions. Using a level set formulation of the free boundary arising in a model for crystal dissolution and precipitation, we are able to apply a formal homogenization procedure to obtain upscaled equations for crystal dissolution and precipitation in a porous medium. For general microscale geometries, the homogenized model is
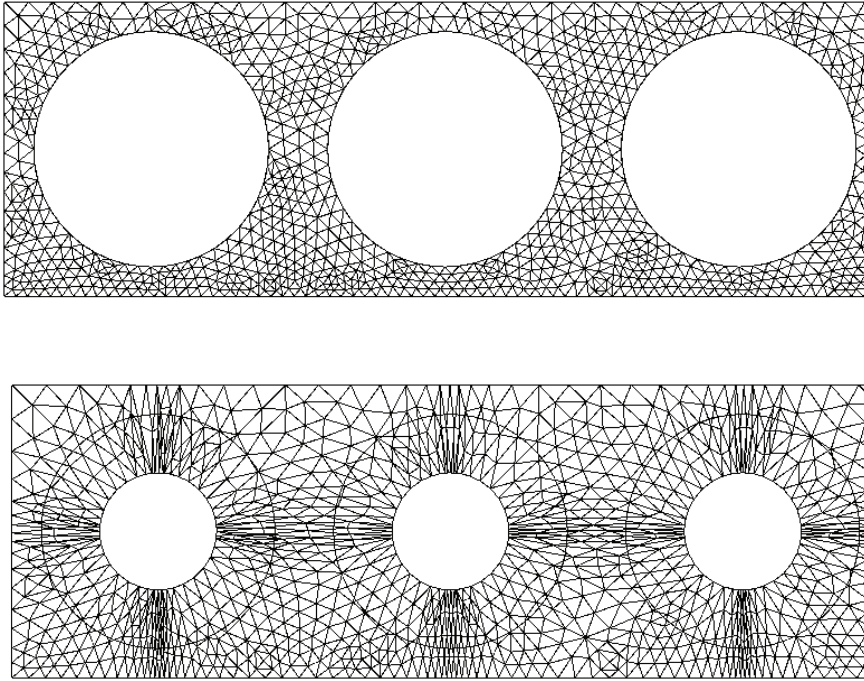
Fig. 4. *The ALE mesh (for a part of the domain) for the initial configuration and for the dissolved configuration.*
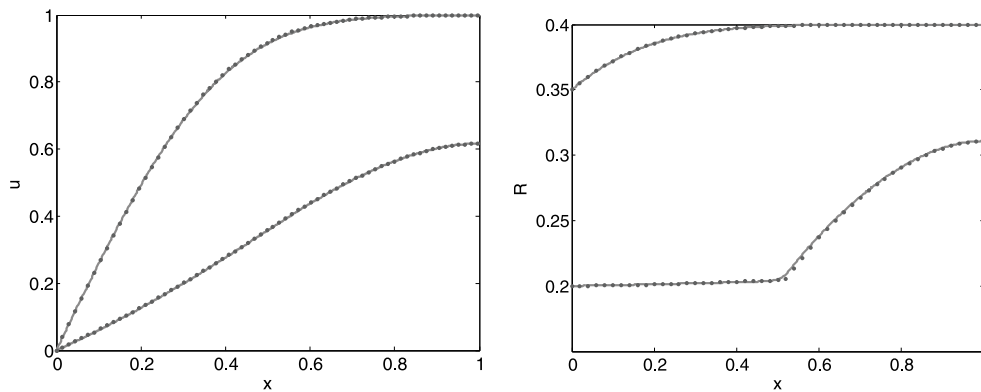

Fig. 5. *Comparison of profiles for $t = 0.05$ and $t = 0.5$. The dots are the microscale model and the line is the homogenized model. In the left plot the concentration u is depicted and in the right plot the radius R.*

a distributed microstructure model. For circular initial inclusions the distributed microstructure model reduces to a system of partial differential equations coupled with an ordinary differential equation. All the unknowns depend only on the slow variable. In order to investigate how well the upscaled equations describe the behavior of the microscale model, we perform numerical computations for a test problem. The nu-

merical simulations show that for the test problem the solution of the homogenized equations agrees very well with the averaged solution of the microscale model.

REFERENCES

[1] COMSOL INC., http://www.comsol.com.
[2] J. DONEA, A. HUERTA, J.-PH. PONTHOT, AND A. RODRÍGUEZ-FERRAN, *Arbitrary Lagrangian–Eulerian methods*, in Encyclopedia of Computational Mechanics, Volume 1: Fundamentals, E. Stein, R. de Borst, and T. J. R. Hughes, eds., John Wiley and Sons, New York, 2004, pp. 413–437.
[3] R. EYMARD, T. GALLOUËT, R. HERBIN, D. HILHORST, AND M. MAINGUY, *Instantaneous and noninstantaneous dissolution: Approximation by the finite volume method*, in Actes du 30ème Congrès d'Analyse Numérique: CANum '98 (Arles, 1998), ESAIM Proc. 6, Soc. Math. Appl. Indust., Paris, 1999, pp. 41–55.
[4] B. FAUGERAS, J. POUSIN, AND F. FONTVIEILLE, *An efficient numerical scheme for precise time integration of a diffusion-dissolution/precipitation chemical system*, Math. Comp., 75 (2006), pp. 209–222.
[5] U. HORNUNG, ED., *Homogenization and Porous Media*, Interdiscip. Appl. Math. 6, Springer-Verlag, New York, 1997.
[6] U. HORNUNG, W. JÄGER, AND A. MIKELIĆ, *Reactive transport through an array of cells with semi-permeable membranes*, RAIRO Modél. Math. Anal. Numér., 28 (1994), pp. 59–94.
[7] P. KNABNER, C. J. VAN DUIJN, AND S. HENGST, *An analysis of crystal dissolution fronts in flows through porous media. Part 1: Compatible boundary conditions*, Adv. in Water Res., 18 (1995), pp. 171–185.
[8] E. MAISSE AND J. POUSIN, *Diffusion and dissolution/precipitation in an open porous reactive medium*, J. Comput. Appl. Math., 82 (1997), pp. 279–290.
[9] S. OSHER AND R. FEDKIW, *Level Set Methods and Dynamic Implicit Surfaces*, Appl. Math. Sci. 153, Springer-Verlag, New York, 2003.
[10] J. A. SETHIAN, *Numerical algorithms for propagating interfaces: Hamilton-Jacobi equations and conservation laws*, J. Differential Geom., 31 (1990), pp. 131–161.
[11] J. A. SETHIAN, *Level Set Methods*, Cambridge Monogr. Appl. Comput. Math. 3, Cambridge University Press, Cambridge, UK, 1996.
[12] A. TARTAKOVSKY, T. SCHEIBE, G. REDDEN, P. MEAKIN, AND Y. FANG, *Smoothed particle hydrodynamics model for reactive transport and mineral precipitation*, in Proceedings of the XVI International Conference on Computational Methods in Water Resources, P. J. Binning, P. K. Engesgaard, H. K. Dahle, G. F. Pinder, and W. G. Gray, eds., Copenhagen, Denmark; also available online from http://proceedings.cmwr-xvi.org.
[13] A. M. TARTAKOVSKY, P. MEAKIN, T. D. SCHEIBE, AND R. M. EICHLER WEST, *Simulations of reactive transport and precipitation with smoothed particle hydrodynamics*, J. Comput. Phys., 222 (2007), pp. 654–672.
[14] C. J. VAN DUIJN, L. A. PELETIER, AND R. J. SCHOTTING, *On the analysis of brine transport in porous media*, European J. Appl. Math., 4 (1993), pp. 271–302.
[15] C. J. VAN DUIJN AND I. S. POP, *Crystal dissolution and precipitation in porous media: Pore scale analysis*, J. Reine Angew. Math., 577 (2004), pp. 171–211.
[16] C. J. VAN DUIJN AND R. J. SCHOTTING, *Brine transport in porous media: On the use of Von Mises and similarity transformations*, Comput. Geosci., 2 (1998), pp. 125–149.
[17] T. L. VAN NOORDEN, *Crystal precipitation and dissolution in a thin strip*, European J. Appl. Math., 20 (2009), pp. 69–91.
[18] T. L. VAN NOORDEN AND I. S. POP, *A Stefan problem modelling dissolution and precipitation*, IMA J. Appl. Math., 73 (2008), pp. 393–411.
[19] T. L. VAN NOORDEN, I. S. POP, AND M. RÖGER, *Crystal dissolution and precipitation in porous media: L^1-contraction and uniqueness*, Discrete Contin. Dyn. Syst., Suppl. (2007), pp. 1013–1020.